PAPER

Check for updates

A novel approach to measure needle insertion responses and the overlooked impact of insertion on injection outcomes

S. Kiana Naghibzadeh,*[a] Hana Rudykh,[a] Brendan M. Unikewicz[b] and Tal Cohen [iD] *[ab]

Needle-based injection techniques are widely used in drug delivery, diagnostics, and soft material characterization, yet the mechanical influence of the insertion process on the ensuing injection behavior remains poorly understood. Here, we demonstrate that both the morphology of the expanded cavity and the resisting pressure are not only governed by material properties, but can be critically influenced, and even reliably modulated, by the preceding needle insertion and retraction processes. To investigate the insertion process, we measure the pressure developed in the droplet that is initially suspended at the tip of the needle and then driven through the material to obtain pressure–depth curves. This offers a local measure of tearing resistance that is not governed by frictional forces along the needle shaft. By systematically varying the insertion and retraction depths and speeds in two contrasting soft materials, we find that features in the pressure–depth curve reliably indicate expected outcomes of the injection procedure, as defined for different use cases. These findings reveal the insertion phase as a critical yet previously underutilized control in drug injection and needle-based mechanical testing, and establishes pressure–depth monitoring as a real-time diagnostic tool. By eliminating reliance on visual confirmation, this approach can improve the robustness, scalability, and automation potential of needle-based injection methods, particularly in opaque, biological, or high-throughput environments.

1 Introduction

Fluid injection, *via* needle-based methods, plays a central role in fields such as drug delivery *via* injection,[1–3] food technology,[4,5] robotic manipulation,[6–8] and in elucidating the mechanical response of a broad range of materials systems ranging from soft material characterization to geotechnical applications.[9–12] Before injecting a fluid, a needle is typically inserted into a deformable material, inducing local deformation and tearing, as well as interfacial effects such as adhesion and friction. Upon injection, various effects can be observed: the fluid can induce cavity expansion; may leak up along the needle shaft; create fracture patterns; or induce a combination of these mechanisms. These different effects can either limit or enhance the success of the injection procedure, depending on the specific application. For example, drug leakage during injection can lead to medical challenges,[13–16] while tissue fracture may enhance absorption

rates. Additionally, needle-based mechanical testing methods, such as needle-induced cavitation rheology (NICR)[10,17] and volume-controlled cavity expansion (VCCE),[9,18] rely on the expansion of a cavity to infer mechanical properties.† However, which of the various injection responses emerges in a particular injection process may seem random, and coupling between needle insertion and subsequent system behavior during injection remains largely underexplored and poorly understood. In fact, needle insertion is often regarded as a preparatory step that has minimal influence on the subsequent behavior of the system.[18–20]

Though several studies have investigated needle insertion characteristics,[1,21–32] little research has been conducted to elucidate their influence on the ensuing injection response. Instead, the primary focus has been on understanding and quantifying puncture forces, tearing energy, tissue damage, and best practices when choosing needle shapes and sizes. Nonetheless, understanding the influence of insertion on injection outcomes can inform drug delivery practices to enhance their precision, and can guide the development of needle-based methods to obtain more reliable and repeatable results. Some

[a] Department of Civil and Environmental Engineering, Massachusetts Institute of Technology, Cambridge, 02139 MA, USA. E-mail: kiana@mit.edu, talco@mit.edu
[b] Department of Mechanical Engineering, Massachusetts Institute of Technology, Cambridge, 02139 MA, USA

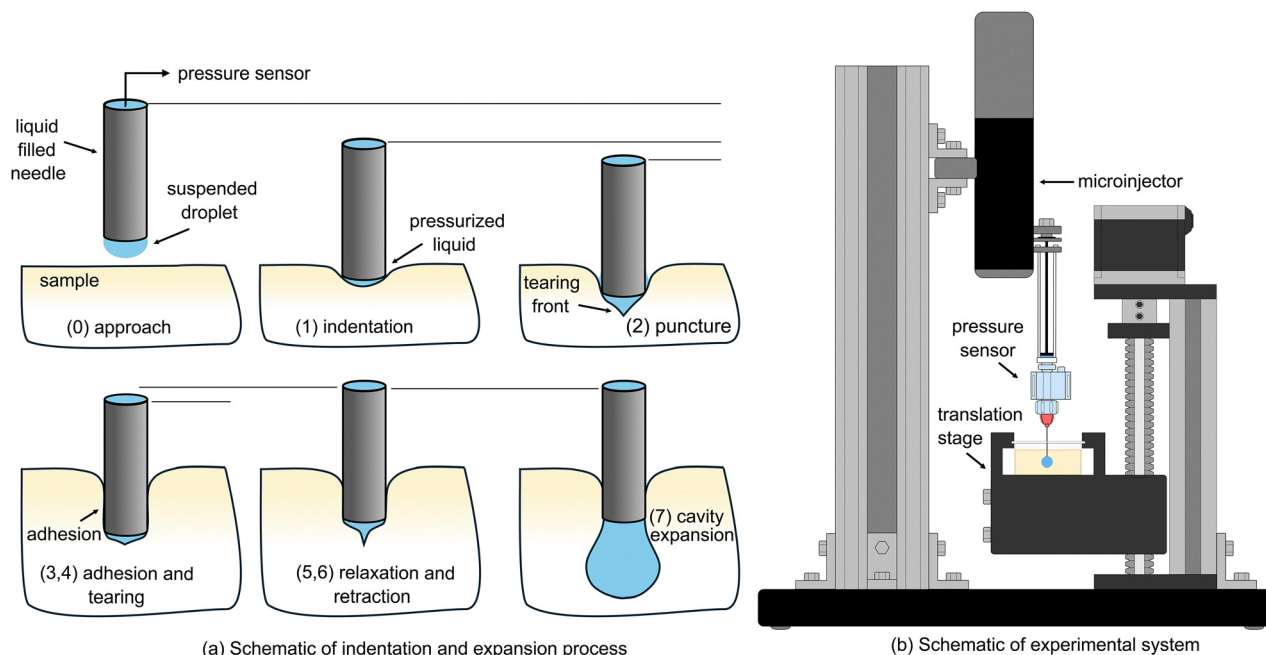† We will refer to these methods as needle-induced methods from here on.

Fig. 1 Experimental process: (a) the key steps of the insertion-injection protocol. (b) The experimental setup used to perform controlled insertion and injection tests within the 1.8-inch acrylic cubes of PDMS or gelatin.

earlier studies already hint toward potential effects; it has been shown, for example, that the insertion speed can impact drug delivery outcomes,[3,33] and that a slight needle retraction prior to injection can alter the measured mechanical properties.[34] However, the absence of a systematic study employing controlled protocols to explain the complete process of insertion and injection hinders our ability to understand the link between these two steps and to investigate if such a link can be utilized to predict or improve the overall success of the injection procedure. This motivates two central questions:

(1) How does the process of needle insertion influence the injection response?

(2) Can insertion protocols be leveraged to improve injection outcomes and their robustness?

A key enabling ingredient in this work, allowing us to answer the above questions, is the development of a method to measure the resisting pressure at the tip of the needle as it is driven through the material *via* a precisely controlled insertion process, as illustrated in Fig. 1. By capturing the pressure in the fluid column that was initially partially suspended as a droplet at the tip of the needle, this measurement yields a pressure-depth curve that characterizes the material's local resistance to penetration. This curve is analogous to the force–displacement response in traditional indentation[24] and deep indentation methods,[27] but has the advantage of removing the confounding effects of surface friction typically associated with force measurements at the indenter base and along the needle.

Using this method, we begin our study by investigating the mechanics of needle insertion using two contrasting soft material formulations: polydimethylsiloxane (PDMS), as a representative of synthetic soft materials,[35] which is an adhesive and tough

material; and gelatin as a representative biological simulant,[36,37] which is a weakly-adhesive material.‡ Our approach involves automated protocols that control the rate and depth of both insertion and retraction of the needle, and then performing controlled injection of an incompressible liquid into the soft solid material. We measure the pressure of the incompressible liquid at the tip of the needle throughout insertion and retraction, *i.e.*, insertion curve, and resisting pressure as a liquid is injected in a volume-controlled fashion, *i.e.*, injection curve. We then analyze the injection curve alongside its respective insertion curve and visualize injection induced morphologies. This direct comparison will reveal that key events during insertion – such as puncture, re-adhesion, tearing, and relaxation – have measurable effects on the injection, specifically, they significantly influence the morphological behavior of the injected fluid, affecting whether the fluid expands to form a cavity, leaks to the surface, or propagates a fracture.

Building on these insights, we offer metrics to improve both the efficiency of injection in drug delivery and the robustness of needle-induced mechanical testing methods. These insights prove to be especially effective for needle-based testing methods such as VCCE, which has shown significant promise in biological applications[35,36,38] and high-throughput testing of mechanical properties in soft materials, which is increasingly in demand with emerging material design methods;[39–41] however, such methods have been limited due to a high-degree of

---

‡ Here, we use the term 'adhesion' in an effective sense to denote the ability of the needle-material interface to maintain a sealnote and sustain negative cavity pressures. This effective sealing behavior arises from a combination of interfacial interactions and the radial stress exerted by the soft material on the needle shaft.

technical proficiency and experience required to perform such experiments.

This manuscript is organized as follows: in the next section we will detail the materials and methods used in this study. Then, in Section 3, we describe the experimental results for both the insertion and the injection responses, showing the observed cavity morphologies and differentiating between typical and atypical pressure curves, we further provide an analysis of the results and their implication in addressing the two aforementioned questions of this work. Finally, we conclude in Section 4.

2 Materials and methods

2.1 Experimental design

We developed a needle-based experimental system that enables precise control over insertion depth, retraction distance, and injected fluid volume into soft materials, allowing us to investigate how needle insertion and retraction influence both the morphology and pressure response during fluid injection.

We adapted an experimental setup from Unikewicz et al.[42] to automate the insertion and retraction protocols before fluid injection (Fig. 1b). The adapted system varies from Unikewicz et al. by employing a RATTMMOTOR EBX1605 CNC Linear Stage Actuator, whereas Unikewicz et al. used a rack-and-pinion mechanism mounted directly on the instrument column, which provided manual, rate-agnostic insertions and placed greater emphasis on quasi-static pressure-zeroing rather than the controlled-rate insertions investigated in this study. The motor operations are managed via a Pololu Tic 36v4 USB controller, powered by a 24 V 8.5 A AC/DC power supply. Motion profiles, i.e. the trajectory of the sample as it is raised and withdrawn from the stationary needle via a velocity-controlled rate, for insertion and injection are programmed through a Python interface in Microsoft Visual Studio Code. Soft material samples were cast into 1.8-inch acrylic cubes and secured on the translation stage with a custom Bambu Lab Polylactic acid filament 3D-printed mount. Injections were performed using a McMaster-Carr 25 Gauge stainless steel dispensing needle with a luer lock connection, 1.00" in length, straight with a blunt tip attached to a 10 μL luer-tipped Hamilton syringe filled with Leakmaster™ leak locating dye and distilled water. Fluid injection was performed at a volumetric flow rate of 600 nL s^{-1} via a World Precision Instruments (WPI) UltraMicroPump3, and WPI MICRO2T, with pressure recorded via a PendoTech PRESS-S-000 sensor connected to an Adafruit NAU7802 24-Bit ADC and read into the laptop computer via a Qwiic connection into an Adafruit Trinkey QT2040 USB Key. Specifically, the pressure sensor operates (without risk of failure) over a measurement range of approximately −80 to 517 kPa (−11.5 to 75 psi). According to the manufacturer, each sensor is tested for accuracy between −69 and 414 kPa (−10 to 60 psi) and is within ±5% of the reading. To reduce variation between tests, the same pressure sensor was used.

The sequence of steps in the insertion and injection procedures is illustrated in Fig. 1(a). Prior to each test, the syringe plunger is adjusted to form an approximate 20 nL fluid cap at the needle tip, eliminating potential air entrapment between the needle and the material surface (step 0). Next, the needle is positioned directly above the sample, with the fluid cap in contact with the material surface. Once in position, the needle is inserted into the soft material at a controlled speed for a prescribed depth (steps 1–4). After insertion, the needle is retracted at a controlled speed over a specified distance (steps 5 and 6) and then allowed to relax for ∼1 minute. Fluid injection is then performed at the prescribed rate of 600 nL s^{-1} for a total fluid volume of approximately 9.2 μL (step 7).

2.1.1 Visualization. To enhance visualization during injection, a concentrated fluorescent leak-locating dye illuminated with 365 nm and 395 nm ultraviolet LEDs was used. Both insertion and fluid injection were captured via a Nikon D90 DSLR camera equipped with an AF-S Micro NIKKOR 105 mm f/2.8G ED lens. The camera was focused on the needle-tip and positioned perpendicular to the sample.

2.2 Material fabrication

In this study, we examine two representative soft materials: PDMS, a characteristic synthetic material for studying the mechanics of soft materials; and gelatin, a natural material representative of biological tissues such as liver.[36] PDMS is adhesive to the needle while gelatin is weakly-adhesive.

2.2.1 PDMS fabrication. Polydimethylsiloxane (PDMS) samples were prepared using a DOW SYLGARD™ 184 silicone elastomer base and curing agent at a base-to-curing agent ratio of 45 : 1 corresponding to an instantaneous shear modulus of approximately 11 kPa.[35] The PDMS components were mixed in 150 mL resin containers and placed within a Thinky SR-500 planetary centrifugal mixer to homogenize the uncured solution. The resulting mixture was poured into 1.8-inch acrylic cubic molds and degassed in a vacuum chamber. Samples were then cured in a convection oven at 60 °C for 4 hours. After oven-curing, the samples were rested at room temperature for 6 days prior to testing.

2.2.2 Gelatin fabrication. Gelatin samples were prepared using Knox™ unflavored gelatin powder and distilled water. The weight ratio of gelatin powder-to-distilled water was 1 : 10 corresponding to an instantaneous shear modulus of approximately 7 kPa.[43] The gelatin powder was first mixed with half the water weight at room temperature, followed by the addition of boiling water to the room temperature solution to fully dissolve the gelatin powder mixture. The solution was manually stirred until uniform and then poured into 1.8-inch acrylic cubic molds. Molds were refrigerated overnight to allow complete gelation. All gelatin tests were conducted the day after casting.

2.3 Experimental test cases

The insertion depth and retraction distance were varied systematically as summarized in Table 1, for both gelatin and PDMS samples.

In all tests, the needle was inserted at one of the three speeds, inspired by existing values in the literature and observed values seen in clinical practice,[44–46] 12.5 mm s^{-1} (fast), 2.5 mm s^{-1} (medium), and 0.5 mm s^{-1} (slow), with a

Table 1 Different cases tested. All depths are in mm

Case IDs	Gelatin		PDMS	
	Insertion	Retraction	Insertion	Retraction
Case 1	15	0	23	5
Case 2	15	1	23	7
Case 3	15	2	23	9
Case 4	15	4	23	12
Case 5	5	0	18	5
Case 6	5	1	18	7
Case 7	1	0	10	5

fixed 1-second dwell time before needle retraction at the same speed as insertion. Each condition was repeated three times per material, resulting in a total of 63 tests per material and 126 tests total. For every test, approximately 9.2 μL of fluorescent leak-locating dye and distilled water was injected at a constant volumetric rate of 600 nL s^{-1}.

3 Results and discussion

In this section, we present the results from 126 experiments conducted on the two materials: gelatin and PDMS.

3.1 Needle insertion response

To analyze how the needle interacts with the material prior to fluid injection, we focus on the pressure–depth (P–δ) curve, which captures the pressure experienced by the incompressible fluid inside the needle as a function of the needle tip's position. This curve provides a non-visual, real-time understanding of what the needle and surrounding material are experiencing during insertion and retraction.

3.1.1 Typical insertion response. A typical pressure–depth response during needle insertion and retraction exhibits six characteristic events (as illustrated in Fig. 1):

(1) Initial surface indentation by the advancing needle,

(2) Surface puncture,

(3) Adhesion of the material to the needle shaft,

(4) Tearing of the material up to the target depth,

(5) Dwelling and stress relaxation period,

(6) Needle retraction to form an initial defect.

These features are consistently observed across both PDMS and gelatin, although the specific curve shapes vary between these contrasting materials. Each event was identified by correlating pressure–depth data with synchronized video recordings. Fig. 2 illustrates representative P–δ curves for both materials, annotated with synchronized images of the needle slightly before puncture§. See the SI for collected insertion and injection curves. Note that although all materials go through these six characteristic events during a 'typical' insertion procedure, the resulting curves may reveal differences between materials, as seen in Fig. 2.

A key distinction between PDMS and gelatin is how the pressure responds at the moment of puncture. In gelatin,
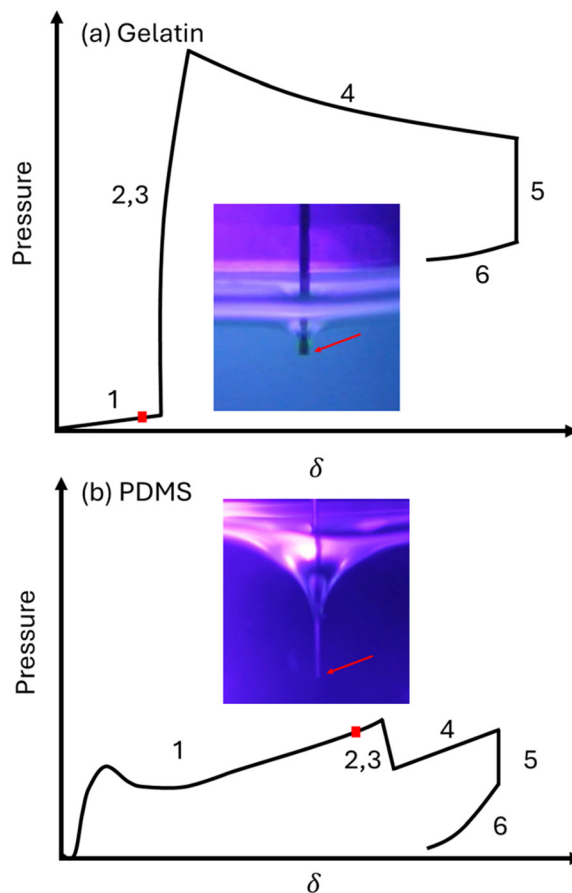
§ Cases with zero retraction (Cases 1, 5, and 7 in Table 1) exhibit only the first four steps.

Fig. 2 Schematic representation of a typical pressure–depth curve during insertion of the needle into (a) gelatin and (b) PDMS. Key events labeled on the curves correspond to those introduced in Section 3.1. The accompanying images show the needle positioned just before puncture (marked with a red dot), highlighting differences in confinement behavior between the two materials. The red arrows in the images indicate the needle tip. The curves are plotted on arbitrary vertical scales to emphasize qualitative differences in the shapes of the insertion and injection responses. Quantitative ranges of the characteristic pressures and their dependence on insertion speed, insertion depth, and retraction length are reported in Sections 3.4 and 3.5 and in the SI.

puncture leads to a sharp rise in pressure, while in PDMS it causes a sudden pressure drop. This contrast arises from the mechanics of fluid confinement at the needle tip. At the start of insertion, the fluid droplet at the tip is unconfined and remains at ambient pressure. As the needle advances, the surrounding material gradually encloses the tip, increasing confinement and raising fluid pressure. In gelatin, puncture typically occurs early, at ∼2 mm and before full confinement, so the fluid becomes suddenly trapped upon puncture, producing a sharp pressure spike. Whereas, PDMS has a much larger insertion depth ∼13 mm and confinement builds gradually, often producing a subtle pressure bump during the initial stages of indentation. When the fully confined tip is released by puncture, the local stress relaxes abruptly, resulting in a sharp pressure drop. This difference in confinement behavior is visually apparent in the overlaid needle images shown in Fig. 2, which capture the state of each material immediately before puncture.

These curves provide a mechanistic fingerprint of needle-material interaction and serve as the foundation for our subsequent analysis. Accordingly, the insertion and retraction values listed in Table 1 were chosen to span distinct regimes of interaction. Insertion depths in Cases 1–6 were selected to ensure puncture, while Case 7 was specifically designed to avoid puncture. Retraction distances were chosen incrementally to remain near or below half the insertion depth.

3.1.2 Atypical pressure drops. While the pressure–depth trajectory described earlier captures the general structure of needle insertion and retraction, many tests exhibited sharp, sudden pressure drops during insertion or retraction, often distinct from puncture or tearing, that deviate from the standard patterns shown in Fig. 2. These drops indicate additional mechanical events.

In PDMS, such drops occurred exclusively during retraction, as shown in Fig. 3, along with images of the needle tip just before and during the pressure drop. These observations suggest that the drop corresponds to the onset of a vacuum-like condition; as the needle separates from the surrounding solid, the initial defect grows large enough so that a confined cavity begins to form, creating negative pressure that attempts to draw fluid out of the needle. When the cavity grows, the adhesion between the needle and PDMS creates a seal, which pulls on liquid from the needle; as a result, the pressure reaches negative values. If retraction is continued into this negative pressure regime, a subsequent pressure rise is observed if the seal is broken. We hypothesize that this pressure rise may result from either fluid cavitation, leading to an air bubble that alleviates the pressure, or material failure, which can occur at the defect site or at the material–needle interface.

In gelatin, however, pressure drops may occur at multiple stages: during puncture, during steady tearing, or during retraction, as shown in the pressure–depth curves of four representative
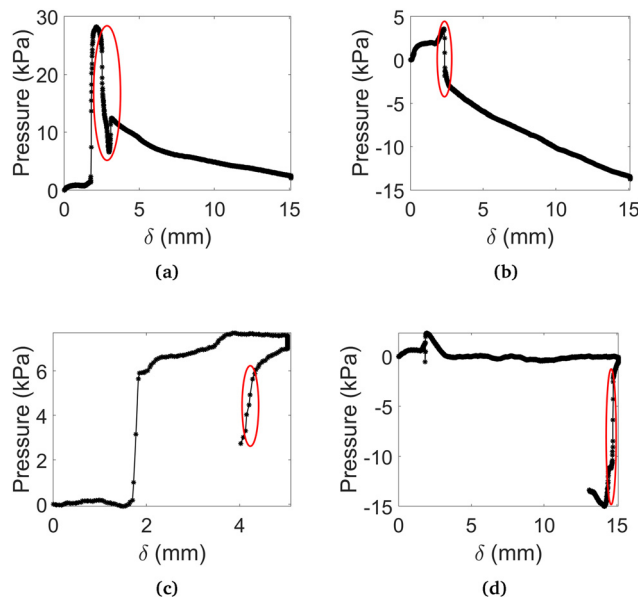

Fig. 4 Representative pressure–depth curves for gelatin that deviate from the typical insertion profile described in Section 3.1. Shown are (a) and (b) Case 1, slow speed showing two typical responses; (c) Case 6, slow speed; and (d) Case 3, medium speed, as defined in Table 1. These curves exhibit irregular pressure drops. No such deviations were observed in tests conducted at fast insertion speeds.

tests in Fig. 4. These drops are frequently followed by surface leakage during fluid injection. In such cases, tension is relieved not through cavity formation but through adhesive failure, allowing the fluid to escape.

In summary, although similar in appearance, sharp pressure drops have fundamentally different implications in PDMS and gelatin. In PDMS, they are mechanical fingerprints of cavity initiation; in gelatin, they serve as early indicators of interface failure, which will be explored further in the next sections.

3.2 Injection patterns

The injected liquid has been observed to follow one or more of three primary modes:

(1) Crawling up the needle shaft,

(2) Expanding into a cavity within the material, and/or

(3) Fracturing the material and propagating through a crack.

The fluid naturally follows the path of least resistance, *i.e.* whichever direction requires the least pressure and energy to displace the surrounding medium. The distinct patterns observed in PDMS and gelatin under various test conditions may be seen in Fig. 5 and 6, respectively.¶

3.2.1 PDMS: stable cavity morphologies. In PDMS, the injected fluid consistently remains confined near the needle tip, forming well-contained cavities, as shown in Fig. 5. The liquid neither crawls up the shaft nor leaks to the surface. This behavior reflects the material's combination of toughness and
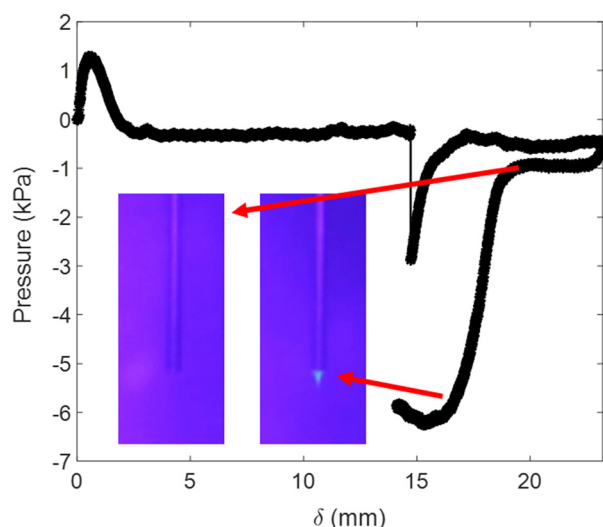

Fig. 3 Representative pressure–depth curve for PDMS showing a sharp pressure drop during retraction in Case 3 of Table 1 (slow insertion). The overlaid images show the needle tip before (top) and after (bottom) the drop, indicating the formation of an initial defect.

¶ Case 7 is excluded here, as it was designed to prevent puncture. In that case, the fluid leaked immediately across the surface without forming a cavity or fracture.
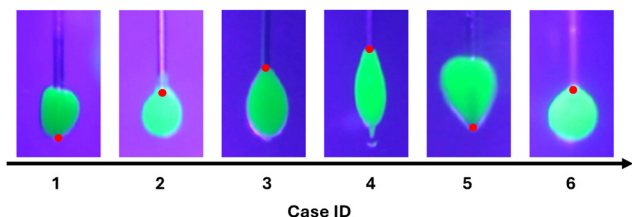
Fig. 5 Injection morphologies in PDMS for Cases 1–6 from Table 1, arranged left to right. Red dots mark the position of the needle tip in each case.
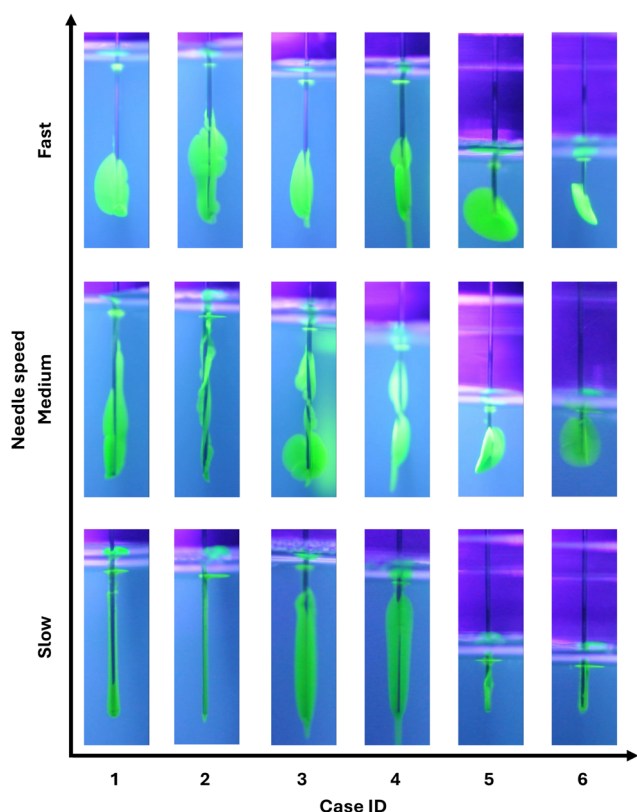

Fig. 6 Injection morphologies in gelatin for Cases 1–6 from Table 1, arranged left to right. The top row shows results from the fastest insertion speed, the middle row corresponds to medium speed, and the bottom row shows the slowest insertion speed within the tested cubic samples.

strong needle adhesion which discourages delamination and promotes compact, low-surface-area morphologies.

Under these conditions, retraction distance becomes the dominant factor in determining cavity shape. Small retractions (Cases 1 and 5) produced cavities that wrapped around the needle shaft with minor upward crawling. Medium retractions (Cases 2 and 3) yielded nearly spherical cavities, while large retractions (Case 4) formed elongated, teardrop-shaped cavities concentrated at the needle tip.

When retraction distances were too small, injection often led to extreme pressure buildup, sometimes exceeding the sensor's limit or causing fluid leakage at system connections. These failures suggest that the system resists delamination even under high stress; rather than peeling along the needle shaft, the fluid

remains confined and forms a pressurized cavity. To prevent such failures, a minimum retraction of 5 mm was used in PDMS tests, as summarized in Table 1. In contrast, insertion depth had minimal effect, and cases with identical retraction but different insertion depths, such as Cases 1 *vs.* 5 and 2 *vs.* 6, resulted in nearly indistinguishable cavity morphologies.

Finally, the insertion and retraction speed made only minor contributions towards the formation of cavities (Fig. 5). Across all tested speeds, patterns remained consistent, suggesting that the PDMS–needle interface is robust and only moderately sensitive to rate effects within the studied range (see the SI) and the location of the injection morphology with respect to the blunt needle tip.

3.2.2 Gelatin: speed-sensitive patterns. In gelatin, the injected fluid often escapes upward along the needle shaft or leaks directly to the surface without forming a well-contained internal cavity or fracture surface. These outcomes reflect the material's weak adhesion to the needle, which allow early delamination and reduce resistance to fluid migration.

As a result, and in contrast to PDMS, insertion and retraction speed had a significant influence on injection behavior. As shown in Fig. 6, at slow speeds, the fluid frequently leaked upward or across the surface (Cases 1, 2, 5, and 6), indicating early adhesive failure and poor confinement. At medium speeds, the fluid formed elongated cavities or fracture surfaces that extended along the needle shaft. At high speeds, confinement improved, producing compact cavities localized near the needle tip.

This trend suggests that faster needle motion limits interfacial fluid infiltration, allowing the gelatin to maintain contact with the needle shaft long enough to constrain the fluid. Similar effects have been reported in agarose gels and biological tissues, where higher insertion speeds enhance interface integrity and reduce both material damage and delamination.[47–49]

In contrast to PDMS, retraction distance had a less pronounced effect in gelatin. In many cases, and particularly at low speeds, fluid migrated along the shaft regardless of retraction value. This behavior underscores the dominant role of adhesion quality over retraction depth in determining the injection pattern.

Finally, a recurring chiral fracture pattern was observed in medium-speed cases. This may result from asymmetric or partial delamination along the needle or from mechanical deformation of the needle during insertion. Regardless of the source, the presence of these consistent patterns highlights gelatin's sensitivity to rate-dependent adhesion and mechanical instability.

3.3 Resisting pressure during injection

To assess how the system resists fluid injection, we analyze the pressure–volume (*P*–*V*) curve, which records injection pressure as a function of injected fluid volume. This curve captures how both the surrounding material and the needle-material interface respond to the expanding cavity as fluid is delivered at a controlled rate.

3.3.1 Typical pressure–volume response. A typical injection response occurs when the fluid remains confined within the

material, forming a cavity or fracture pattern without leaking to the surface. In these situations, the pressure–volume curve follows a reproducible trend with three distinct phases:

(1) Elastic expansion: pressure rises as the material resists the initial deformation caused by the expanding fluid volume.

(2) Fracture initiation: a peak occurs when the material yields or fractures in response to the internal stress.

(3) Post-fracture behavior: as additional fluid is injected, the pressure may drop or plateau, reflecting continued cavity growth or crack propagation with reduced resistance.

Representative pressure–volume curves for both gelatin and PDMS are shown in Fig. 7. See the SI for all collected gelatin and PDMS injection curves.

The difference in the pressure–volume curves for gelatin and PDMS reflects their inherent material properties. PDMS, being tough and elastic, undergoes a smooth transition into fracture, with a gradual pressure decline. In contrast, gelatin exhibits more brittle behavior, with a sharp pressure drop following fracture. These responses are consistent with prior VCCE studies and are commonly used to extract material properties using models of cavitation or large-strain elasticity.[9,36] Additionally, the peak pressure, often referred to as the critical pressure, is used in needle-induced cavitation methods (NICR) to characterize material properties.[17]

3.3.2 Atypical pressure–volume responses. Not all injection responses followed the typical curve described in the previous section. In several cases, the pressure–volume curve deviated from the expected pattern, indicating that the measured pressure arose from factors other than the material's mechanical resistance. These atypical responses appeared in different forms depending on the material and interaction conditions:

• Leaking: this behavior is common in gelatin, particularly at low insertion speeds. Deviations in the pressure–volume curve occur when the injected fluid leaks to the surface instead of remaining confined within the material. The resulting curves (Fig. 8) deviate from the typical form and are dominated by the flow resistance of fluid escaping along the needle shaft, rather than by the material's mechanical resistance.

• Improper initial defect: as discussed in Section 3.2, in PDMS leaking is of lesser concern, however, not all the pressure–volume curves are similar to the typical curve. This is
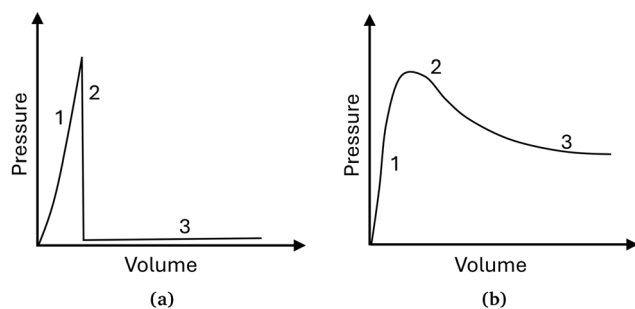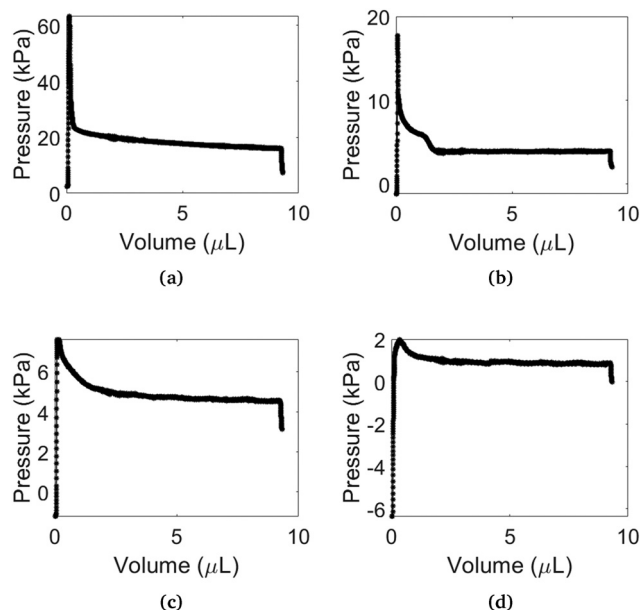

Fig. 8 Representative pressure–volume curves for selected tests in gelatin where fluid leakage was observed. These plots correspond to the pressure–depth curves shown in Fig. 4, presented in the same order.

because a very small initial defect will lead to the presence of enhanced resistance during injection. With a large initial defect, the injected liquid mainly fills up the cavity and smaller deformation to the surrounding solid is required. Fig. 9 demonstrates these two extremes where the pressure–volume curve deviates from the standard one together with their associated
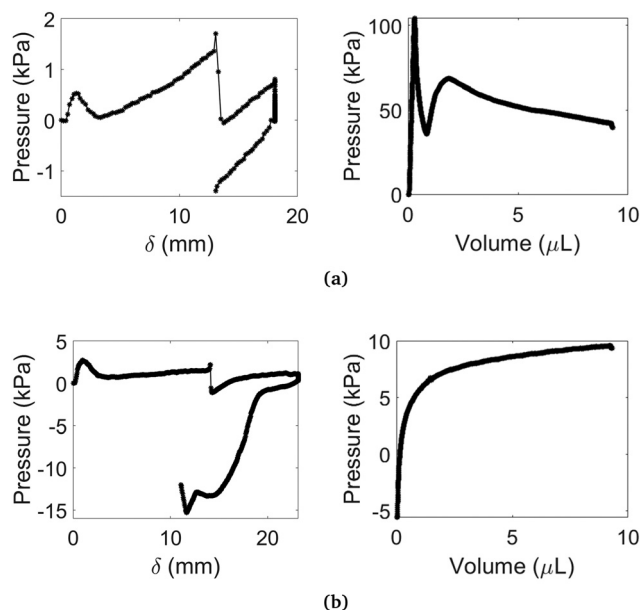

Fig. 9 Representative injection behavior in PDMS for cases with (a) too small retraction (Case 5, fast speed) and (b) too large retraction (Case 4, medium speed), as defined in Table 1. The left panels show the corresponding pressure–depth curves during insertion and retraction, while the right panels show the pressure–volume curves during injection.

Fig. 7 Schematic representation of a typical pressure–volume (P–V) curve observed during injection for (a) gelatin and (b) PDMS. Key events labeled on the curves correspond to those introduced in Section 3.3.

pressure–depth curve. A highly confined defect results in double-peaked curves due to excessive resistance to fluid injection (Fig. 9a, right), while a large pre-formed void allows the fluid to fill the cavity without fully engaging the surrounding material, producing monotonic curves dominated by volume filling (Fig. 9b, right). In both cases, the pressure response is not primarily governed by the material's bulk resistance.

• No puncture: when the needle failed to puncture the surface (*e.g.*, Case 7), the injected fluid remained near the surface or intermittently escaped into the surrounding space. The resulting pressure–volume curves (Fig. 10) did not follow the typical trend and showed inconsistent or non-standard behavior, differing from successful injection responses.

The results presented in this study highlight the critical role of needle motion in shaping system behavior during fluid injection into soft materials. We performed tests in two contrasting materials: PDMS, representing a tough, synthetic elastomer, and gelatin, serving as a simplified simulant for biological tissue.

A key finding is that the morphology of the injected fluid is highly sensitive to the needle's insertion and retraction profile, even when the material and injection rate are held constant. While simplified, gelatin mimics key characteristics of biological tissues and has been widely used as a tissue simulant in prior studies.[37] As such, the results observed in gelatin may offer insight into tissue-level injection responses. This has important implications for applications such as drug delivery. In particular, the geometry of the injected volume and its contact area with the surrounding tissue can significantly influence drug absorption and uptake. A larger fluid–tissue interface may promote more effective therapeutic outcomes, whereas leakage along the needle shaft reduces delivery efficiency. This is particularly relevant in clinical contexts where drug leakage is a frequently reported issue

during injection.[14–16] Additionally, as seen in Fig. 3, we observed a secondary rise in insertion pressure in some PDMS tests following the initial pressure drop associated with defect initiation. We hypothesize that this may result from bubble formation within the needle or the system, which temporarily impedes flow and increases resistance. If similar behavior were to occur during needle retraction in biological tissue—particularly prior to injection—it could result in unintended localized air injection, posing risks in clinical contexts.

Another key finding of this study is the influence of needle insertion on the pressure–volume response during injection—an effect that has direct implications for needle-induced material testing methods, which are increasingly used to characterize the mechanical behavior of soft materials. In volume-controlled cavity expansion (VCCE), an incompressible liquid is injected into the bulk of a material at a controlled rate, under the assumption that the injection leads to the formation and expansion of a cavity. The injected volume and corresponding pressure are recorded to produce a pressure–volume curve, which is typically analyzed using models of cavitation to extract material properties. Similarly, in needle-induced cavitation rheology (NICR), the maximum pressure during fluid injection is used in conjunction with theoretical cavitation models to estimate material parameters.

However, both techniques are susceptible to failure modes such as surface leakage, improper initial defect formation, or incomplete puncture. These conditions can distort the pressure–volume response and lead to inaccurate or invalid mechanical measurements. Currently, such failures are often diagnosed through visual observation, *e.g.*, by monitoring for leakage or verifying needle placement, but reliance on visual cues limits the broader applicability of these methods, particularly in opaque materials, *in vivo* experiments, or high-throughput testing environments where direct observation is not feasible.

Building on the insights developed in the previous section, we now discuss how characteristic features of the pressure–depth curve, recorded during needle insertion and retraction, provide a reliable and quantitative alternative to visual monitoring. In many cases, these curves can serve as real-time diagnostic tools, enabling assessment of test validity and identification of failure modes, even in the absence of visual access.

Fig. 10 Representative pressure–depth (left) and pressure–volume (right) curves for Case 7 from Table 1, showing non-puncture behavior in (a) gelatin and (b) PDMS.

3.4 Faster insertion decreases the chance of leaking in gelatin and potentially in biological tissues

A frequent failure mode in drug injection and needle-induced testing methods, especially in weakly-adhesive materials like gelatin and biological tissues, is leakage of the injected fluid along the needle shaft to the surface. In such cases the efficacy of the injection declines; and in needle-induced testing methods, the pressure–volume curve becomes unreliable, as the measured pressure no longer reflects the material's resistance to internal deformation.

As shown in Section 3.2, insertion speed is a decisive factor in avoiding this failure. At slow speeds, the gelatin–needle interface fails to maintain adhesion, allowing fluid to escape. At high speeds, adhesion is preserved, enabling the fluid to remain confined and a cavity or fracture surface to form.
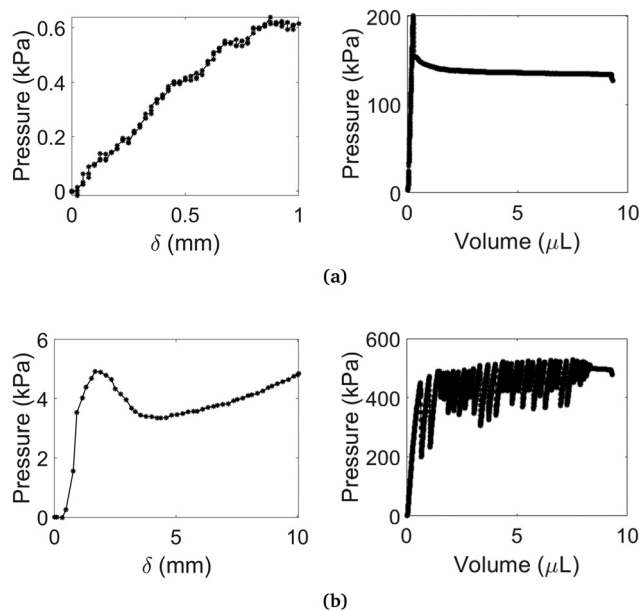
This trend is mirrored in the pressure–volume behavior: faster insertion results in higher critical pressures during insertion and injection, as shown in Fig. 11 and 12. This increase in critical pressure with speed reflects improved confinement at the interface. At low speeds, weak adhesion allows fluid to bypass the material by delaminating the interface, facing minimal resistance. At higher speeds, the fluid must deform the surrounding solid, leading to higher pressures. Notably, our analysis found no significant correlation between critical pressure and retraction depth prior to puncture or leakage (see the SI).

The pressure–depth curves discussed in Section 3.1 reinforce this interpretation. Tests that leaked consistently exhibited a sharp pressure drop during insertion or retraction (Fig. 4), indicating interface failure. In contrast, tests with smooth, monotonic pressure–depth curves (similar to Fig. 2) led to successful cavity formation and interpretable pressure–volume data (as seen in the SI). The impact of insertion speed is summarized in Table 2: at slow speeds, leakage occurred in over 80% of tests; at fast speeds, leakage was completely eliminated.

These findings provide a simple, actionable guideline: to minimize leakage and ensure injection efficiency and test validity in soft, weakly-adhesive materials, faster insertion speeds are favorable, even without changes to the injection protocol. Furthermore, the pressure–depth curve offers a built-in diagnostic for failure: when a sharp drop occurs during insertion or retraction, it signals interfacial adhesion failure and a high likelihood of leakage. This is particularly valuable in needle-induced testing for *in vivo* or high-throughput settings where visual confirmation is not feasible.

In model systems like gelatin, it is possible to compare the pressure–volume response to a known "ground truth" and recognize when a test fails. However, in more complex
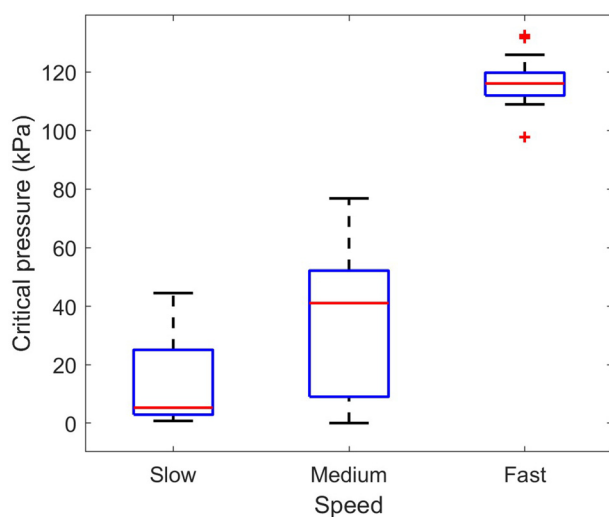

Fig. 12 Fluid injection critical pressure variations in gelatin as a function of insertion speed (0.5 mm s^{-1} (slow), 2.5 mm s^{-1} (medium), and 12.5 mm s^{-1} (fast)). Box plots represent the distribution of critical pressure values across all valid tests at each speed. For each box, the central line indicates the median, the box bounds show the interquartile range (25th–75th percentile), and the whiskers extend to the minimum and maximum values within 1.5 times the interquartile range. Individual points outside this range are plotted as outliers.

Table 2 Percentage of tests exhibiting leakage during injection in gelatin at different insertion speeds, out of 18 tests conducted per speed group. Case 7 of Table 1 (non-puncture) was excluded from the analysis

Speed	Leaked (%)
Slow	83.3
Medium	16.6
Fast	0

materials, such as biological tissues being characterized with needle-induced testing methods for the first time, such reference curves do not exist. In these cases, pressure–volume data alone cannot confirm test validity. Instead, real-time metrics derived from the pressure–depth curve become essential.

3.5 Deviation in pressure–volume curve for PDMS

Injected fluid in PDMS consistently expands into a confined cavity near the needle tip, rather than migrating along the shaft as seen in gelatin. As a result, leakage is not a primary failure mode in PDMS. However, the shape and quality of the formed cavity are highly sensitive to retraction distance, which governs both the size of the initial cavity before injection and the shape of the final cavity after injection. Furthermore, although other phenomena (*e.g.*, lateral cracking[50,51]) have been reported in the literature, we have not seen evidence of this in our experiments.

As discussed in Section 3.3, this morphological dependence is reflected in the pressure–volume curves. When the retraction distance is well-tuned, the resulting cavity enables a pressure–volume response that closely follows the typical curve in Fig. 7. In contrast, very small retractions cause the injected fluid meeting high resistance (Fig. 9a). Conversely, excessive retractions create

Fig. 11 Needle insertion critical pressure variations in gelatin as a function of speed (0.5 mm s^{-1} (slow), 2.5 mm s^{-1} (medium), and 12.5 mm s^{-1} (fast)). Box plots represent the distribution of critical pressure values across all valid tests at each retraction level. For each box, the central line indicates the median, the box bounds show the interquartile range (25th–75th percentile), and the whiskers extend to the minimum and maximum values within 1.5 times the interquartile range. Points outside this range are plotted individually as outliers.
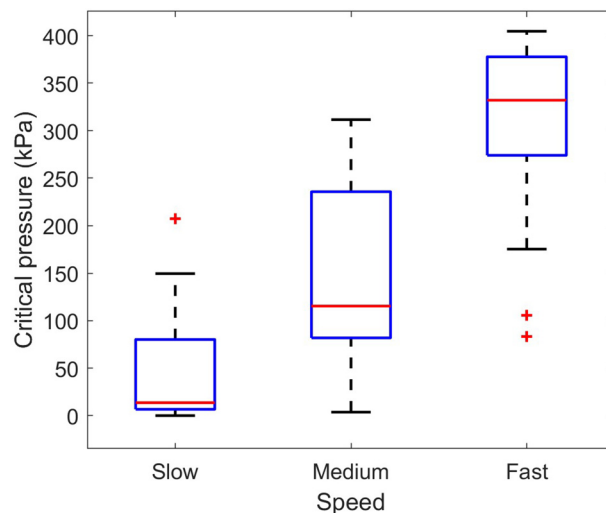
large, pre-formed cylindrical voids that the fluid fills without significantly deforming the material (Fig. 9b). In both extremes, the pressure–volume data cannot be reliably used to extract material properties in needle-induced testing methods.

This trend is further supported by the data in Fig. 13 and 14, which shows that needle insertion critical pressures vary slightly with the insertion rate for PDMS; however, critical pressures during fluid injection varied significantly as a function of the retracted distance of the needle from insertion processes. Larger cavities accommodate more fluid before material resistance is engaged, resulting in lower peak pressures. Smaller cavities resist expansion earlier, producing higher critical pressures. However, across all retraction values, the strong adhesion between PDMS and the needle prevents delamination, leaving material deformation as the primary mechanism governing the injection response. Consistent with this trend, critical pressure showed minimal correlation with the insertion or retraction speed in PDMS (Fig. 13), reinforcing that interface behavior is not the dominant factor in PDMS.

These observations suggest the existence of an optimal retraction range that produces an initial cavity of suitable size. However, the retraction distance alone is not a reliable predictor of success: both small (5 mm) and large (12 mm) retractions sometimes led to valid or invalid pressure–volume responses. Instead, we found that the pressure–depth curve offers a more consistent and interpretable signature of cavity quality.

As described in Section 3.1, a sharp pressure drop during retraction indicates the onset of cavity nucleation, typically followed by a gradual pressure rise as the cavity expands and fluid continues to be drawn from the needle. The most reliable pressure–volume behavior occurred when retraction ended
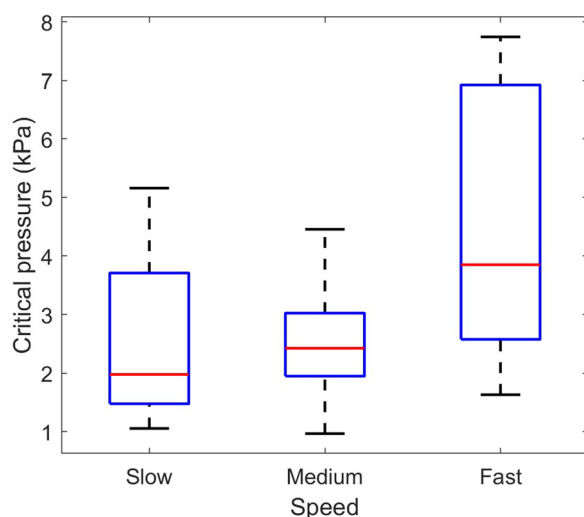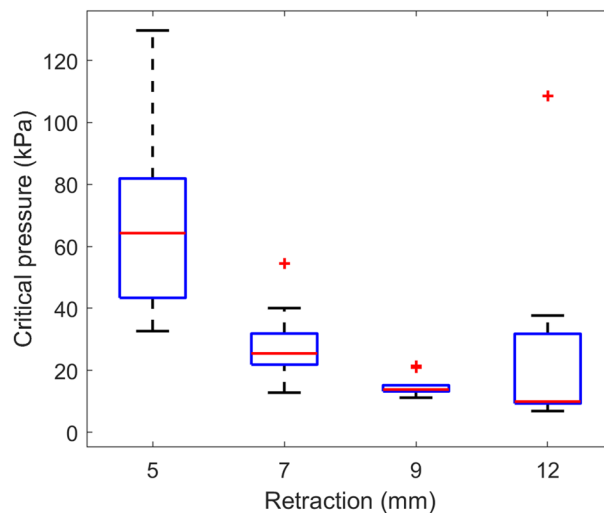

Fig. 14 Fluid injection critical pressure variations in PDMS as a function of retraction depth. Box plots represent the distribution of critical pressure values across all valid tests at each retraction level. For each box, the central line indicates the median, the box bounds show the interquartile range (25th–75th percentile), and the whiskers extend to the minimum and maximum values within 1.5 times the interquartile range. Points outside this range are plotted individually as outliers.

during this drop—after the pressure began to fall, but before it began rising again introducing air bubble in the system. This simple criterion accurately predicted successful outcomes in approximately 80% of the 54 PDMS tests performed (excluding Case 7, in which puncture did not occur).

This result not only provides a real-time, quantitative diagnostic for cavity formation, but also may connect to practices used in related methods. In NICR, a critical retraction distance is often defined to minimize residual stress before injection.[34] Similarly, pressure-zeroing has been adopted as a retraction endpoint in prior PDMS VCCE studies.[42]

3.6 Identifying puncture

In both clinical settings and needle-induced testing methods, a valid injection requires that the needle punctures the surface and reaches the bulk of the material before fluid injection begins. If puncture fails, the injected fluid remains outside or trapped near the surface, and the resulting pressure no longer reflects the material's bulk mechanical response. Identifying whether puncture has occurred is therefore essential for determining injection validity. Puncture is typically confirmed through visual observation. However, this method is not scalable or feasible in cases where injections target inner tissue layers, requiring multiple barriers to be punctured, or when working with opaque materials, *in vivo* settings, or automated systems. To address this, we use the pressure–depth curve as a non-visual diagnostic tool.

As shown in Fig. 2, tests that fail to exhibit events 2 and 3 in the pressure–depth curve, corresponding to surface puncture and re-adhesion, can be confidently classified as non-puncture cases. This interpretation is supported by results from Case 7 in Table 1, which was explicitly designed to avoid puncture. In these tests, the insertion portion of the pressure–depth curves

Fig. 13 Needle insertion critical pressure variations in PDMS during needle insertion as a function of speed (0.5 mm s^{-1} (slow), 2.5 mm s^{-1} (medium), and 12.5 mm s^{-1} (fast)). Box plots represent the distribution of critical pressure values across all valid tests at each retraction level. For each box, the central line indicates the median, the box bounds show the interquartile range (25th–75th percentile), and the whiskers extend to the minimum and maximum values within 1.5 times the interquartile range. Points outside this range are plotted individually as outliers.

for both gelatin and PDMS show no sharp features, indicating the absence of puncture (Fig. 10, left column).

The corresponding pressure–volume curves (Fig. 10, right column) further support this diagnosis. In PDMS, non-puncture cases produce injection curves that deviate significantly from the standard cavity-expansion behavior (Fig. 7b). The pressure rises erratically and oscillates, due to the fluid intermittently breaking through the confined tip and shooting back toward the surface. In gelatin and potentially biological tissues, the differences are more subtle. Non-puncture injection curves closely resemble those of valid tests, with deviations primarily in the post-fracture region. This makes it difficult to identify puncture failure from injection data alone (Fig. 7a).

These findings highlight the value of using a combination of pressure–depth and pressure–volume data. In well-characterized materials, failed tests may be distinguishable by deviations in injection behavior. Nonetheless, in new or complex systems, especially biological tissues where no baseline response exists, the pressure–depth curve offers a critical, real-time tool for detecting puncture without relying on visual confirmation.

4 Conclusions

This study demonstrates that the morphology of the injected fluid and the pressure required for injection, beyond reflecting material properties, are strongly influenced by how the needle is inserted and retracted prior to injection, a step that is often overlooked. We explored this material response to needle insertion in two contrasting materials: PDMS, a tough, and adhesive elastomer, and gelatin, a weakly-adhesive hydrogel. In PDMS, delaminating the needle from the surrounding material and introducing water between them requires substantial energy, making cavity expansion the preferred pathway. As a result, the geometry and quality of the initial defect, determined by retraction, are critical. In contrast, gelatin's weak adhesion to the needle makes adhesion failure much more likely, and the injected fluid may more easily migrate along the needle shaft. Here, insertion speed plays a central role: fast motion promotes transient adhesion and helps confine the injected fluid near the needle tip, while slow motion leads to early delamination and surface leakage.

Across both materials, we found that the pressure–depth curve provides a real-time, non-visual window into the evolving needle-material interaction. It captures key mechanical events such as surface puncture, cavity nucleation, and adhesion loss, and can be used to anticipate injection outcomes. In the context of needle-based VCCE testing, these features serve as practical diagnostic tools to flag malformed cavities, identify puncture failure, and avoid misleading pressure–volume curves—all without relying on visual confirmation. Hence, they can enable automation of needle-based mechanical testing methods.

Overall, this work underscores the critical and often overlooked role of insertion mechanics in shaping the outcomes of fluid injection. By providing both a mechanistic framework and a diagnostic strategy for improving the reliability of needle-based testing methods, it paves the way for the development of more efficient injection-based drug delivery methods as well as robust and scalable testing of soft materials. Future studies may extend this framework to sharp needles and relevant soft materials, such as brain, thyroid, or liver, to quantify their responses and thereby provide a basis for designing improved injection procedures across different applications.

Conflicts of interest

There are no conflicts to declare.

Data availability

Supplementary information (SI) is available. See DOI: https://doi.org/10.1039/d5sm01023c.

The datasets generated and analyzed during this study are available for download at the Cohen Mechanics Group GitHub: https://github.com/cohen-mechanics-group/soft-matter-insertion-and-injection/.

Acknowledgements

References

1 O. A. Shergold and N. A. Fleck, *Proc. R. Soc. London, Ser. A*, 2004, **460**, 3037–3058.

2 N. Mohaghegh, A. Ahari, F. Zehtabi, C. Buttles, S. Davani, H. Hoang, K. Tseng, B. Zamanian, S. Khosravi and A. Daniali, *et al.*, *Acta Biomater.*, 2023, **172**, 67–91.

3 L. Crawford, J. Rosch and D. Putnam, *J. Controlled Release*, 2016, **240**, 251–266.

4 D. Kim, Y. Cao, D. Mariappan, M. S. Bono Jr, A. J. Hart and B. Marelli, *Adv. Funct. Mater.*, 2021, **31**, 2005370.

5 Z. Faraji Rad, *Adv. Eng. Mater.*, 2023, **25**, 2201194.

6 K. Yang, X. Jin, Z. Wang, Y. Fang, Z. Li, Z. Yang, J. Cong, Y. Yang, Y. Huang and L. Wang, *BMC Ophthalmol.*, 2022, **22**, 484.

7 L. Lindenroth, S. Bano, A. Stilli, J. G. Manjaly and D. Stoyanov, *IEEE Rob. Autom. Lett.*, 2021, **6**, 871–878.

8 S. Misra, K. B. Reed, B. W. Schafer, K. Ramesh and A. M. Okamura, *Int. J. Robot. Res.*, 2010, **29**, 1640–1660.

9 S. Raayai-Ardakani, Z. Chen, D. R. Earl and T. Cohen, *Soft Matter*, 2019, **15**, 381–392.

10 S. B. Hutchens, S. Fakhouri and A. J. Crosby, *Soft Matter*, 2016, **12**, 2557–2566.

11 N. J. O'Keeffe, H. E. Huppert and P. Linden, *J. Fluid Mech.*, 2018, **844**, 435–458.

12 C.-Y. Lai, Z. Zheng, E. Dressaire and H. A. Stone, *Philos. Trans. R. Soc., A*, 2016, **374**, 20150425.

13 D. Yin, J. Forsayeth and K. S. Bankiewicz, *J. Neurosci. Methods*, 2010, **187**, 46–51.

14 G. Spollett, S. V. Edelman, P. Mehner, C. Walter and A. Penfornis, *Diabetes Educ.*, 2016, **42**, 379–394.

15 K. A. Præstmark, B. Stallknecht, M. L. Jensen, T. Sparre, N. B. Madsen and J. Kildegaard, *J. Diabetes Sci. Technol.*, 2016, **10**, 914–922.

16 L. Heinemann, T. Nguyen, T. S. Bailey, A. Hassoun, B. Kulzer, T. Oliveria, Y. Reznik, H. W. de Valk and J. K. Mader, *J. Diabetes Sci. Technol.*, 2023, **17**, 449–457.

17 J. A. Zimberlin, N. Sanabria-DeLong, G. N. Tew and A. J. Crosby, *Soft Matter*, 2007, **3**, 763–767.

18 S. Chockalingam, C. Roth, T. Henzel and T. Cohen, *J. Mech. Phys. Solids*, 2021, **146**, 104172.

19 Z. Song and S. Cai, *Extreme Mech. Lett.*, 2022, **52**, 101673.

20 M. P. Milner and S. B. Hutchens, *Mech. Mater.*, 2021, **154**, 103741.

21 K. Patel and P. Hutapea, *Proc. Inst. Mech. Eng., Part H*, 2023, **237**, 1061–1071.

22 N. Abolhassani, R. Patel and M. Moallem, *Med. Eng. Phys.*, 2007, **29**, 413–431.

23 S. Jiang, P. Li, Y. Yu, J. Liu and Z. Yang, *J. Biomech.*, 2014, **47**, 3344–3353.

24 D. He, D. Malu and Y. Hu, *Appl. Mech. Rev.*, 2024, **76**, 050802.

25 A. Samani and D. Plewes, *Phys. Med. Biol.*, 2007, **52**, 1247.

26 S. Budday, R. Nay, R. De Rooij, P. Steinmann, T. Wyrobek, T. C. Ovaert and E. Kuhl, *J. Mech. Behav. Biomed. Mater.*, 2015, **46**, 318–330.

27 S. Fakhouri, S. B. Hutchens and A. J. Crosby, *Soft Matter*, 2015, **11**, 4723–4730.

28 C. W. Barney, C. Chen and A. J. Crosby, *Soft Matter*, 2021, **17**, 5574–5580.

29 S. Fregonese and M. Bacca, *Soft Matter*, 2022, **18**, 6882–6887.

30 B. A. Goda, Z. Ma, S. Fregonese and M. Bacca, *Soft Matter*, 2024, **20**, 6016–6022.

31 M. Scali, P. Breedveld and D. Dodou, *Sci. Rep.*, 2019, **9**, 19988.

32 S. Fregonese and M. Bacca, *J. Mech. Phys. Solids*, 2021, **154**, 104497.

33 J. N. Mehta, M. K. Rausch and C. G. Rylander, *Int. J. Numer. Methods Biomed. Eng.*, 2022, **38**, e3635.

34 C. W. Barney, Y. Zheng, S. Wu, S. Cai and A. J. Crosby, *Soft Matter*, 2019, **15**, 7390–7397.

35 H. Varner and T. Cohen, *Soft Matter*, 2024, **20**, 9174–9183.

36 H. M. Varner, S. Naghibzadeh, K. Spaeth, A. Klein and T. Cohen, *Exp. Mech.*, 2024, 1–15.

37 A. Leibinger, A. E. Forte, Z. Tan, M. J. Oldfield, F. Beyrau, D. Dini and F. Rodriguez y Baena, *Ann. Biomed. Eng.*, 2016, **44**, 2442–2452.

38 H. Varner, G. P. Sugerman, M. K. Rausch and T. Cohen, *J. Mech. Behav. Biomed. Mater.*, 2023, **143**, 105901.

39 J. E. Griffith, Y. Chen, Q. Liu, Q. Wang, J. J. Richards, D. Tullman-Ercek, K. R. Shull and M. Wang, *Mater. Horiz.*, 2023, **10**, 97–106.

40 Y. Ding, H. Tang, C. Zhang, W. Li, G. Li, Y. Zhang, C. Xu, F. Zhao, Q. Guo and C. F. Guo, *et al.*, *Adv. Funct. Mater.*, 2021, **31**, 2100489.

41 X. Li, B. Unikewicz, S. Chockalingam, H. B. da Rocha and T. Cohen, *arXiv*, 2025, preprint, arXiv:2503.15631, DOI: 10.48550/arXiv.2503.15631.

42 B. M. Unikewicz, A. M. Pincot and T. Cohen, *Rev. Sci. Instrum.*, 2025, **96**, 045109.

43 J. E. Bonavia, *arXiv*, 2025, preprint, arXiv:2512.20502, DOI: 10.48550/arXiv.2512.20502.

44 S. P. DiMaio and S. E. Salcudean, Proceedings 10th Symposium on Haptic Interfaces for Virtual Environment and Teleoperator Systems. HAPTICS 2002, 2002, pp. 344–351.

45 F. Casanova, P. R. Carney and M. Sarntinoranont, *J. Neurosci. Methods*, 2014, **237**, 79–89.

46 S. Okazawa, R. Ebrahimi, J. Chuang, S. E. Salcudean and R. Rohling, *IEEE/ASME Trans. Mechatron.*, 2005, **10**, 285–296.

47 F. Casanova, P. R. Carney and M. Sarntinoranont, *J. Biomech Eng.*, 2012, **134**(4), 041006.

48 M. Mahvash and P. E. Dupont, *IEEE Trans. Biomed. Eng.*, 2009, **57**, 934–943.

49 C. Bjornsson, S. J. Oh, Y. Al-Kofahi, Y. Lim, K. Smith, J. Turner, S. De, B. Roysam, W. Shain and S. J. Kim, *J. Neural Eng.*, 2006, **3**, 196.

50 S. Das and A. Ghatak, *J. Mater. Sci.*, 2011, **46**, 2895–2904.

51 M. Muthukumar, M. Bobji and K. Simha, *Soft Matter*, 2021, **17**, 2823–2831.